Supplemental Figures S1-S5

Johansson et al: A patient derived cell atlas informs precision targeting of glioblastoma

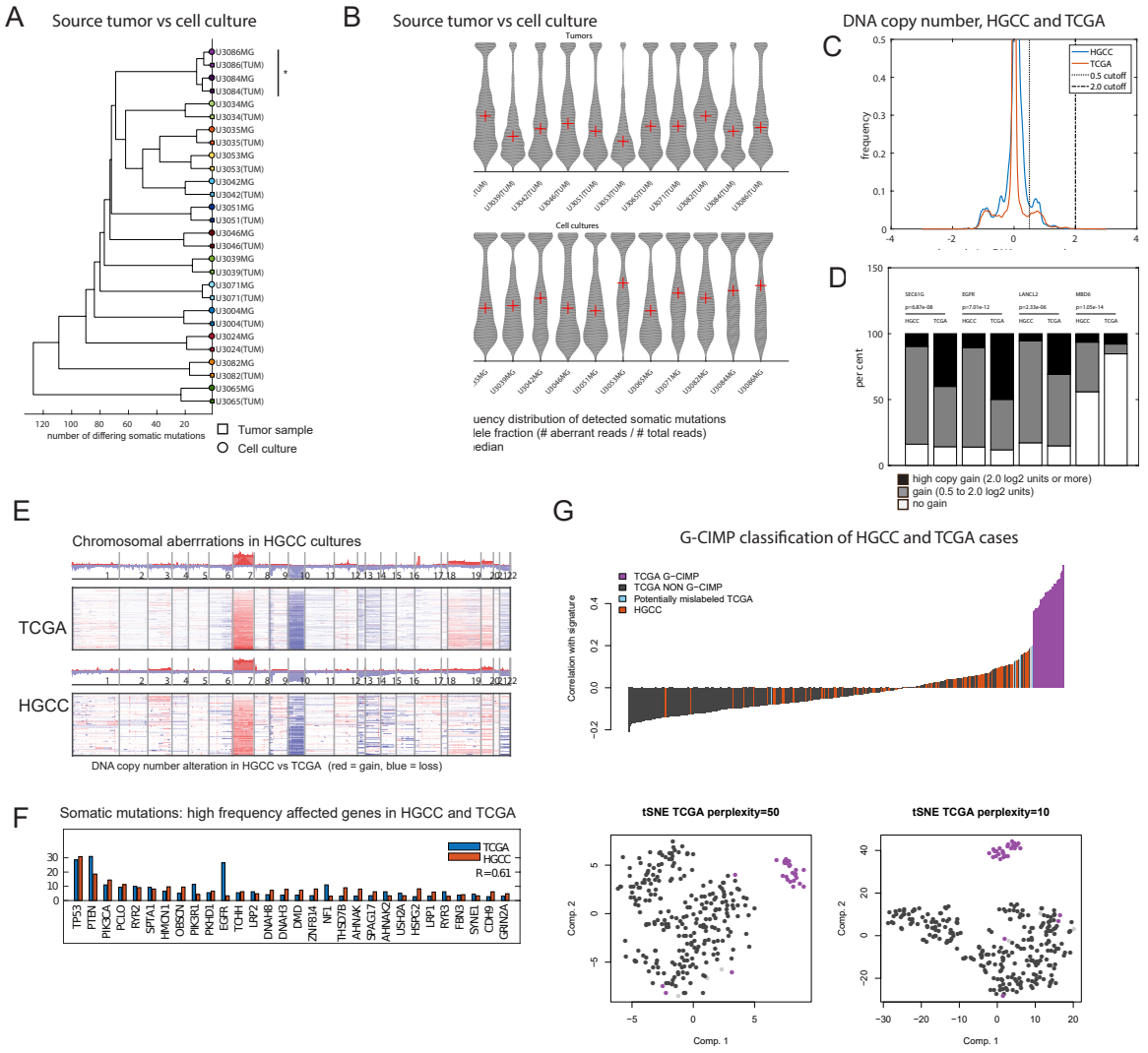

Figure S1: Genomic profiling of the primary GBM cultures. Related to Figure 1. (A) Whole-exome sequencing: similarity of our primary GBM cell cultures (here denoted as the HGCC cohort) to their source tumor (n=14). The tree shows the number of divergent somatic mutations between all samples. The GBM cultures match their corresponding source tumor. (B) histograms of variant allele frequencies in cell cultures and their matched source tumor counterparts (n=14). (C) histograms of DNA copy number aberrations for all hg19 gene loci for our primary culture (HGCC) and TCGA cohorts, respectively, showing 0.5 and 2.0 log units as cutoffs for DNA copy number gains and high-copy amplifications, respectively. (D) 4 genes show significant evidence of differential frequencies of DNA copy gain in HGCC and TCGA (nominal Chi-square p-value $<10^{-6}$). 3 of the genes are in or near the EGFR locus which is less frequently amplified in HGCC than in TCGA. A fourth gene, MBD6 on chr12 had higher gain frequency in HGCC. (E) DNA copy number profiles indicate that the HGCC cultures have a characteristic set of chromosomal lesions. (F) Mutation frequencies of frequently mutated genes show correlated frequencies in HGCC and TCGA (R=0.61).(G) G-CIMP signatures in HGCC and TCGA. First, tSNE analysis of TCGA data highlights a clear separation between G-CIMP and non-G-CIMP cases, with a few observations showing potential mislabeling (Bottom figures). The top 2000 differentially methylated probes between G-CIMP and non-G-CIMP cases in the TCGA were used to derive a G-CIMP signature. The top figure shows per-sample correlation with the G-CIMP signature, clearly identifying the G-CIMP cases in the TCGA. No HGCC cases are clearly G-CIMP.

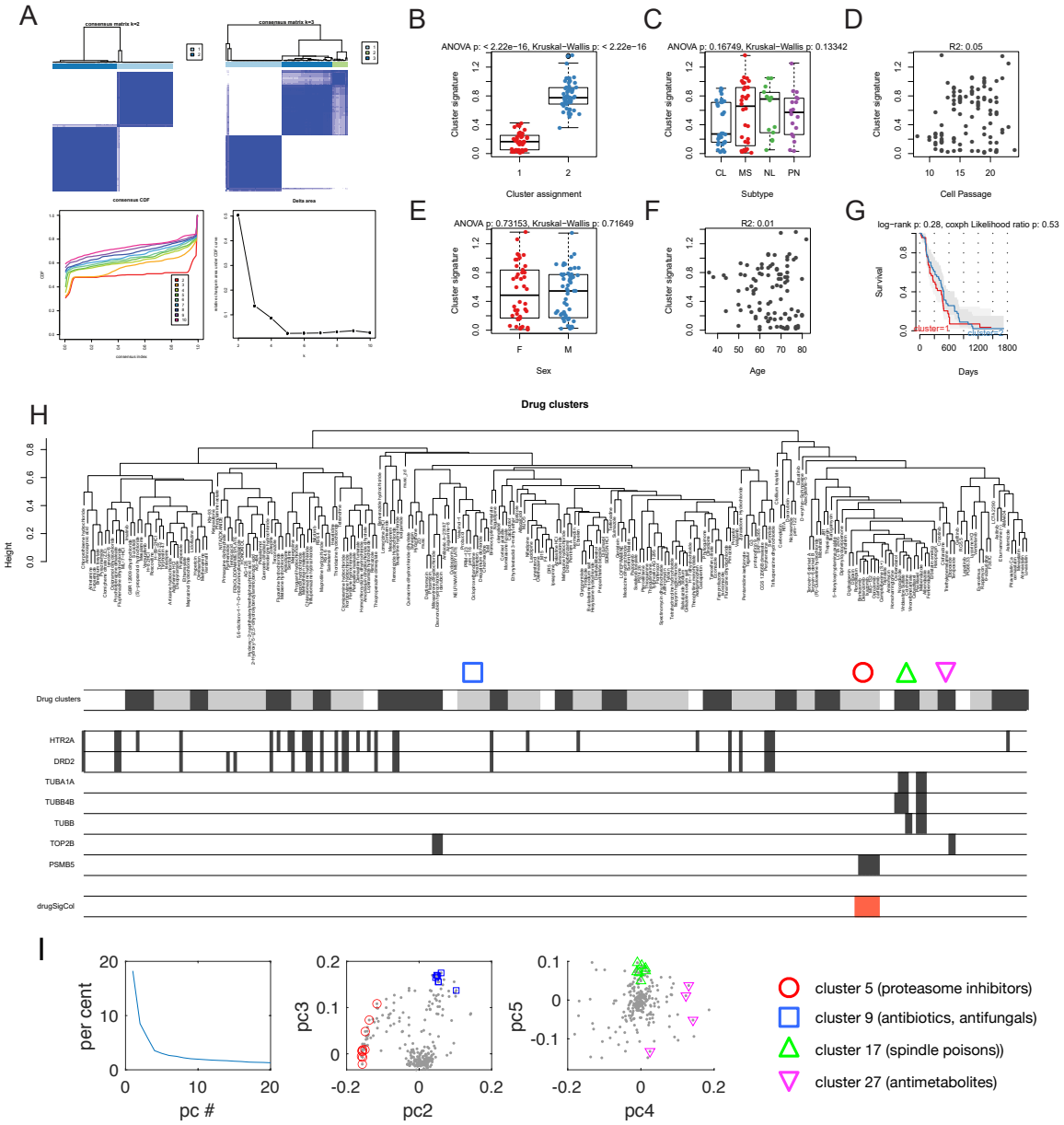

Figure S2: Clustering of drug effects in primary glioblastoma cell cultures. Related to Figure 2.

(A) Diagnostics plots for consensus clustering of HGCC cultures for, supporting that two (2) main clusters of cell cultures are found.
(B-G) Based on the two clusters, we derived a signature (Methods) based on which each cell culture was scored (y-axis, values close to 0 indicate proteasome inhibitor sensitive, close to 1 indicate proteasome inhibitor resistant type glioblastoma). The signature score was not readily explained by (C) transcriptional subtype, (D) cell passage (E) patient sex, (F) patient age, nor (G) postoperative survival.
(H) Clusters of compounds as defined by the dynamic tree cut algorithm (see main text). The cluster number of each compound is also provided in Table S2.

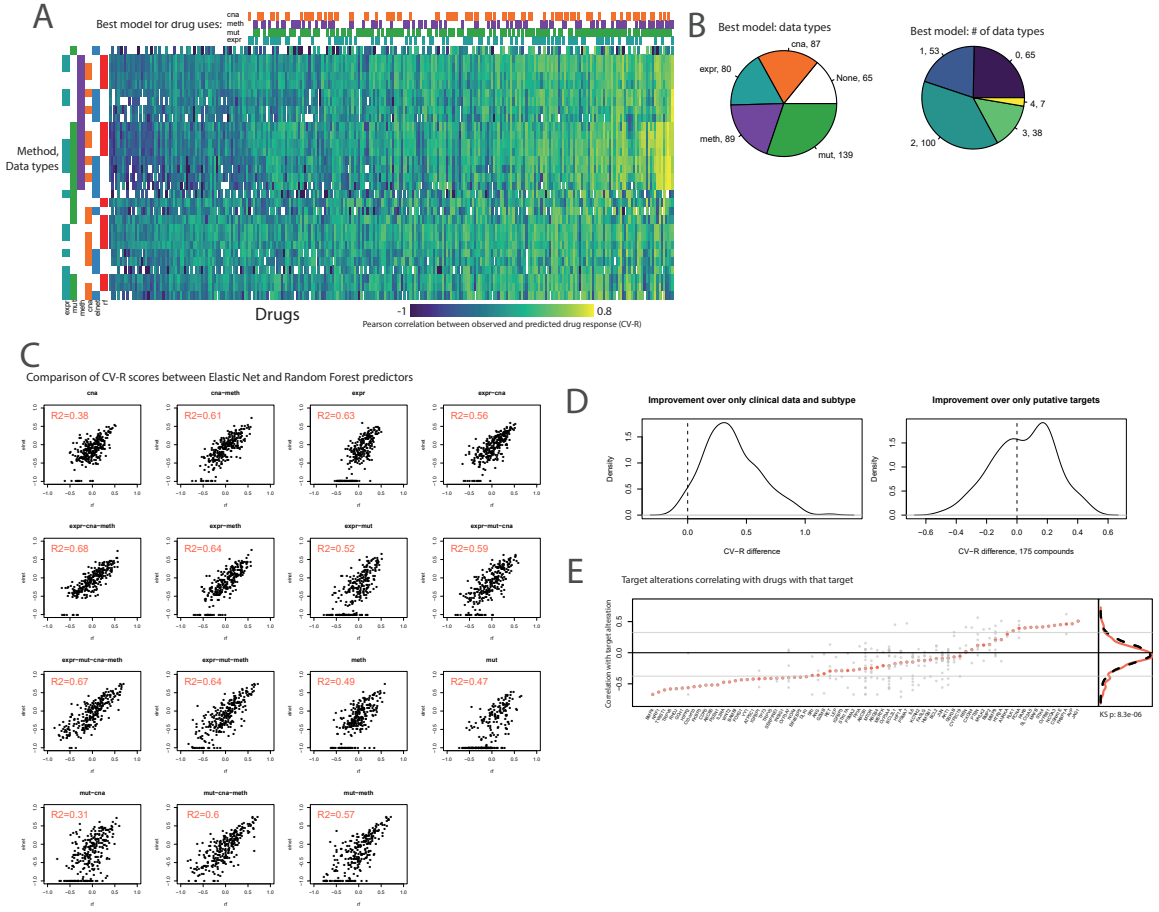

Figure S3: Prediction performance: impact of prediction method and covariate data. Related to Figure 3.

(A) Heatmap of prediction performance (CV-R) for all drugs (columns) and different combinations of prediction method and included data types (rows) (indicated to the left of heatmap). Above the heatmap, the data types included in the highest-scoring model for each drug are indicated.
(B) Types of data and the number of data types included in the set of best models for each drug.
(C) Left: improvement of prediction performance CV-R when using multiple genomic datasets as predictors, relative to using clinical data and transcriptional subtype alone. Right: change of prediction performance CV-R when using multiple genomic data sets as predictors, relative to genomic data sets filtered for STITCH targets.
(D) Comparison of prediction performance obtained with the elastic net and random forest predictors, indicates that there is a very similar performance between the two methods. Points are individual compounds.
(E) evaluation of the correlation between compound effect and the alteration of compound targets. (We operationally defined a gene as altered if it was (i) differentially expressed, (ii) copy number altered at the coding locus, or (iii) has a somatic mutation detected by whole-exome sequencing. We assigned targets to gene products using the STITCH database; score >700).

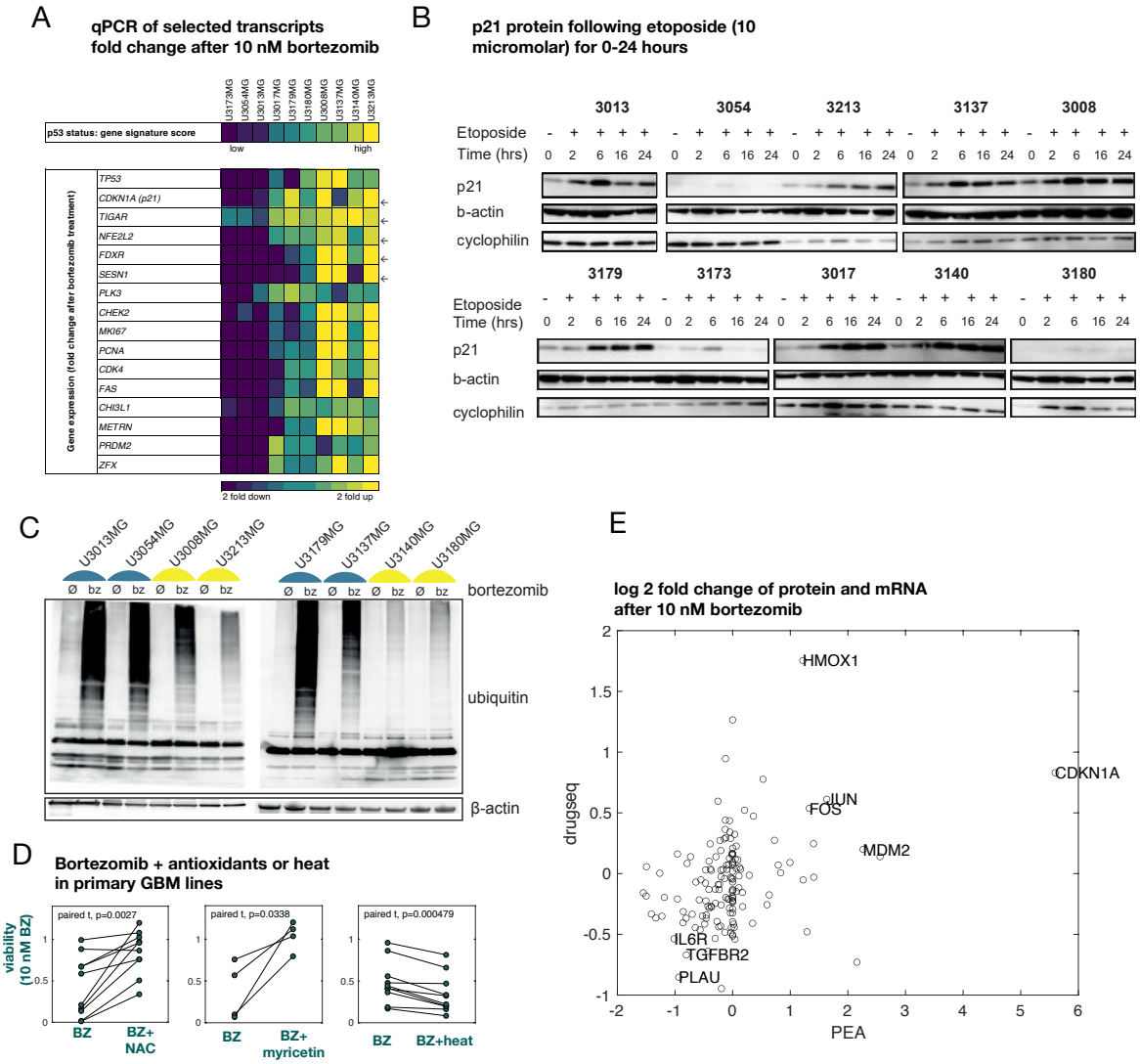

Figure S4: Characterization of PI+ and PI- type glioblastoma cultures. Related to Figure 4.

(A) Gene expression-based signature of p53 activity in primary GBM cells. Genetic status of p53 and the *CDKN2A/B* locus and protein expression is indicated by grey bars showing that the cell line has p53 mutation, *CDKN2A/B* loss or expression of the p21 protein, respectively. Response to p53 reactivating drugs and bortezomib is shown as percent viability. Lower panel shows the relative expression of a panel of genes involved in p53-dependent ROS response, DNA damage response, proliferation, and apoptosis.
(B) Induction of p21 protein in 10 GBM cell cultures, after etoposide treatment, used to probe the function of the p53-p21 pathway. The absence of induction is taken as an indication of reduced/absent p53 activity. (See main text)
(C) Western blot probed with antibodies detecting ubiquitinated proteins, in GBM cells that are sensitive (blue) vs resistant (yellow) to bortezomib
(D) Modulation of proteasome inhibitor response by reducing oxidative stress with antioxidants or aggravating the phenotype by proteotoxic stress using heat in combination with bortezomib treatment (n=10) GBM cell lines, grouped by resistance (5 sensitive vs 5 resistant).
(E) Differential protein expression in bortezomib treated (n=4) GBM cell lines, comparing two p53-mutant sensitive (U3013MG, U3054MG) vs two p53 wildtype resistant lines at baseline and after treatment, respectively. A total of 192 proteins were measured using the proximity extension analysis assay (shown on the x-axis) and plotted against a transcriptional read-out in one sensitive and one resistant line (shown on the y-axis). High induction of *CDKN1A* encoding p21 is indicated both at the transcriptional and the protein level.

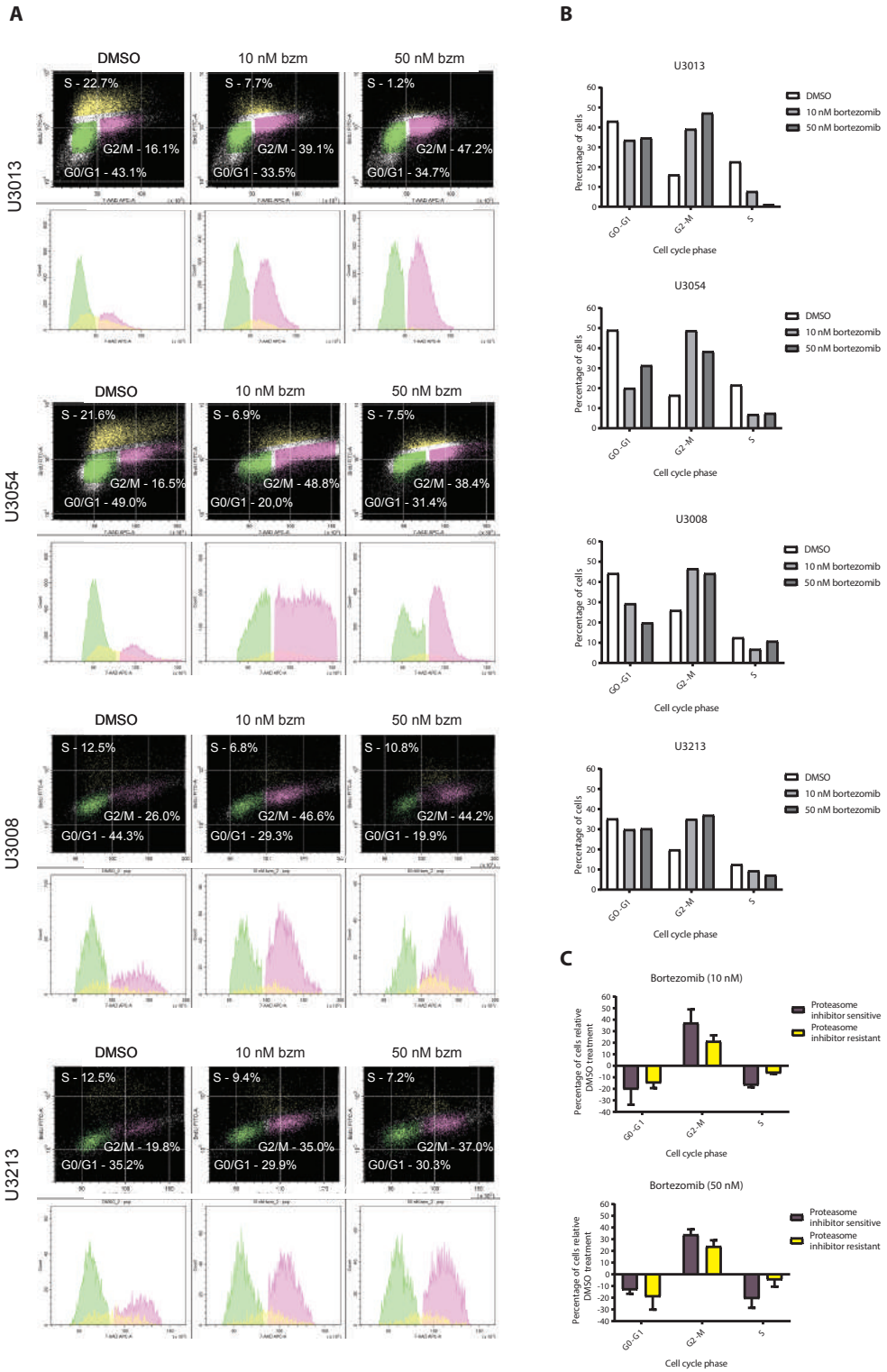

Figure S5: BrdU cell cycle distribution analysis of bortezomib treated GBM cultures.

(A) The plots depict BrdU-FITC / 7-AAD-APC staining patterns and cell cycle histograms generated from the bortezomib sensitive GBM cultures U3013 and U3054 in comparison to the bortezomib resistant GBM cultures U3008 and U3213 following treatment with DMSO, 10- or 50 nM bortezomib respectively.
(B) Percentage of cells in the G0/G1, G2/M and S cell cycle phases.
(C) Percent change in cell cycle phase distribution relative DMSO treated control cells. Mean with standard deviation of two proteasome inhibitor sensitive cultures (U3013 and U3054) and two proteasome resistant cultures (U3008 and U3213) is plotted.